Article | Received 27 March 2026; Revised 23 April 2026; Accepted 11 May 2026; Published 8 June 2026
https://doi.org/10.55092/interdiscipline20260001

Data-driven optimization of screen-printing parameters for thick-film resistors using GA-BP prediction and CPSO search

Yu Sun[1,2,†], Youyang Wang[1,2,†], Jiani Xue[1,2], Xingyao Zhang[1,2], Xiyi Liao[3] and Wenhua Gu[1,2,*]

[1] School of Integrated Circuits (School of Microelectronics), Nanjing University of Science and Technology, Nanjing, China

[2] Ministry of Education Key Laboratory of Near-Range RF Sensing ICs & Microsystems, Nanjing University of Science and Technology, Nanjing, China

[3] 24th Research Institute of China Electronics Technology Group Corporation, Chongqing, China

† These authors contributed equally to this work.

* Correspondence author; E-mail: guwenhua@njust.edu.cn.

Highlights:

- A data-driven GA-BP model enables high-accuracy resistance prediction of thick-film resistors.
- CPSO is employed to achieve efficient global optimization of screen-printing process parameters.
- Significant reduction in resistance error and enhancement of resistance consistency are achieved.

Abstract: Thick-film resistors are widely used in electronic systems, where resistance accuracy and stability are critical for device performance. However, the screen-printing process involves complex multi-parameter coupling, and conventional optimization methods rely heavily on empirical adjustments, leading to low efficiency and limited precision. To address these issues, a data-driven process optimization method is proposed. It combines a genetic algorithm-optimized backpropagation (GA-BP) neural network with a chaotic particle swarm optimization (CPSO) algorithm. A resistance prediction model is constructed using production-line data to capture the nonlinear relationship between process parameters and resistance. The CPSO algorithm is further employed to achieve target-oriented inverse design of process parameters. The results show that the model achieves an R^2 of 0.991 and a mean absolute percentage error below 3.09% on the test set. The optimized parameters reduce the resistance error by up to 14.86%, with the deviations controlled within 5%. These results demonstrate that the proposed method improves the accuracy of process parameter optimization compared with the traditional experience-driven approach.

Keywords: thick-film resistor; screen printing; genetic algorithm; backpropagation neural network; chaotic particle swarm optimization

1. Introduction

Thick-film resistors are widely used in hybrid integrated circuits, radio-frequency and microwave modules, and power electronic systems due to their low manufacturing cost and excellent compatibility with ceramic substrates [1–5]. The stability and consistency of resistor performance directly affect the gain characteristics, noise performance, and overall reliability of the circuit system, making them crucial passive components for achieving circuit impedance matching, bias control, and signal stabilization [6–9]. Therefore, it is crucial to precisely control the resistance value of thick-film resistors during the manufacturing process.

As shown in Figure 1, a typical thick-film resistor consists of an alumina substrate, a resistive film formed by resistive paste, and silver-palladium electrodes, with main fabrication processes of screen printing, high-temperature sintering, and laser trimming [10]. Among these processes, screen printing has become one of the most widely used manufacturing methods in printed electronics because of its good adaptability to various substrates and high process stability. Figure 2 illustrates the screen structure. Specifically, under the pressure of a squeegee, electronic paste is deposited onto the substrate surface through openings in a patterned screen stencil to form the desired resistive pattern [11]. Therefore, the quality of screen printing has a decisive influence on the morphology and thickness of the resistive film [12]. The screen printing process involves multiple key process parameters, including printing pressure, printing gap, printing speed, and screen mesh count. These parameters jointly determine the deposition state of the paste on the substrate, thereby affecting the film thickness, geometry, and final resistance value of the thick-film resistor. Therefore, the rational control of screen printing process parameters has become a key issue in the manufacturing of thick-film resistors.

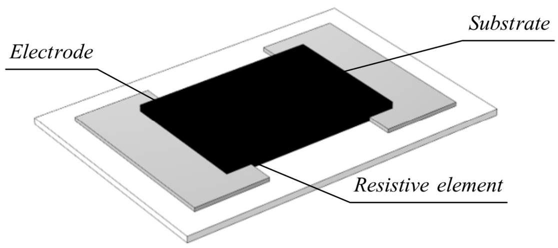

Figure 1. Schematic diagram of the thick-film resistor structure.

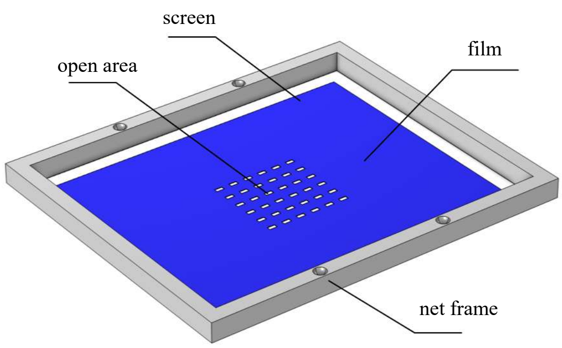

Figure 2. Schematic diagram of the screen structure.

In practice, the optimization of screen printing process parameters is typically based on expert experience and trial-and-error methods [13–17]. However, this experience-driven approach often requires multiple rounds of trial production and parameter adjustments, which not only increases production costs but also reduces production efficiency. Furthermore, because of the strong nonlinear relationships and multi-parameter coupling among screen-printing variables, conventional empirical methods struggle to describe the mapping from process parameters to resistance values accurately, thereby limiting optimization efficiency and accuracy.

In recent years, with the development of data-driven methods, machine learning techniques have shown great potential in the fields of complex process modeling and optimization [18–22]. Mohamad *et al.* proposed a particle swarm optimization–backpropagation neural network (PSO-BP) model for rock strength estimation and demonstrated that particle swarm optimization can improve the predictive performance of backpropagation neural networks in complex engineering problems [23]. Zhu *et al.* compared genetic algorithm–backpropagation neural network (GA-BP), PSO-BP, and conventional BP models for rainfall-induced landslide risk assessment, showing that optimization-assisted BP models achieve higher prediction accuracy than the initial BP network [24]. Shariati *et al.* developed an artificial neural network–particle swarm optimization hybrid model to predict the behavior of channel shear connectors embedded in concrete and verified the effectiveness of combining neural networks with intelligent optimization algorithms for nonlinear engineering prediction tasks [25]. By establishing prediction models using historical production data, machine learning methods can effectively capture the nonlinear relationships between process parameters and device performance and provide a reliable basis for process optimization decisions. Therefore, introducing machine learning methods into the modeling and parameter optimization of the screen-printing process for thick-film resistors is expected to improve resistance prediction accuracy and reduce the number of production debugging iterations, thereby enhancing production efficiency and product consistency.

This paper proposes a screen-printing process optimization method for thick-film resistors by combining machine learning prediction and intelligent optimization algorithms. Specifically, a resistance prediction model for thick-film resistors is first constructed based on a GA-BP neural network, which achieves high-precision modeling of the nonlinear relationship between screen-printing process parameters and resistance values. Then, a chaotic particle swarm optimization (CPSO) algorithm is introduced to perform a global search for screen-printing process parameters and obtain the optimal parameter combination that meets the target resistance requirement. Extensive experiments conducted on a real production line validate the effectiveness of the proposed method. Results show that the proposed resistance prediction model can achieve a mean absolute percentage error (MAPE) as low as 3.09%. Furthermore, the proposed process optimization method can intelligently recommend screen-printing process parameters under given target resistance conditions. Compared with the traditional scheme, the proposed method reduces the resistance error by up to 14.86% and achieves a resistance standard deviation of 2.1 Ω at a target resistance of 115 Ω. Finally, the influence of different screen-printing process parameters on the resistance value is also analyzed.

2. Methodology

In this study, a GA-BP model is adopted as the resistance prediction model for thick-film resistors, and a CPSO algorithm is employed to search the optimal screen-printing process parameter window automatically. In the prediction stage, key process parameters, including printing pressure, printing gap, and printing speed, are taken as input variables, while the resistance value is taken as the output. GA-BP is used to establish the nonlinear mapping relationship. Specifically, the BP neural network is used for function approximation, whereas the GA is used to optimize the initial weights and thresholds of the network, thereby improving model convergence performance and avoiding entrapment in local optima. On this basis, the optimization of the screen-printing process parameter window is further carried out. The CPSO algorithm is introduced for the process parameter optimization problem under a given target resistance value, and the trained GA-BP model is used as the fitness function. The process parameters are treated as optimization variables, and a global search is performed within the design space. By introducing a chaotic mapping mechanism to enhance particle swarm diversity, the global search capability of the algorithm is effectively improved, and premature convergence is suppressed. Through the above method, efficient optimization of the screen-printing process parameter combination under the target resistance requirement is achieved.

2.1. GA-BP model for thick-film resistance prediction

Considering the characteristics of multi-parameter coupling, complex influence relationships on resistance performance, and strong nonlinearity in the screen-printing process of thick-film resistors, it is difficult for traditional empirical models or analytical methods to achieve high-accuracy prediction. Therefore, a BP neural network is introduced in this study to construct a nonlinear mapping model between process parameters and performance indicators. The BP neural network has strong function approximation capability and can adaptively learn complex input–output relationships through a multilayer structure [26], thereby enabling effective prediction of thick-film resistor performance.

However, in practical applications, BP neural networks are highly sensitive to initial weights and thresholds and are prone to becoming trapped in local optima, which leads to degraded model generalization performance. This problem is particularly pronounced when the distribution of process parameters is uneven or the number of samples is limited. To address the above limitations, GA is introduced to perform global optimization of the key parameters of the BP neural network [27]. Through a population-based search mechanism, the genetic algorithm performs global optimization in the parameter space and can effectively avoid the local convergence problem associated with traditional gradient descent methods. Specifically, the GA is used to optimize the initial weight and threshold distribution of the BP neural network, so that the network is located in a relatively favorable region of the solution space at the early stage of training, thereby improving the convergence speed and prediction accuracy of the model. Under the same network structure and training conditions, compared with the conventional BP model, the GA-BP model exhibits stronger robustness and higher prediction accuracy when dealing with the dataset of thick-film resistor process parameters. The overall algorithm flow of the proposed GA-BP method for thick-film resistance prediction is summarized in Algorithm 1.

Algorithm 1 GA-BP hybrid algorithm for thick-film resistance prediction.

Input: Dataset $\{(X_i, R_i)\}_{i=1}^{N}$, GA parameters ($T_{\max}, cr, pm, \alpha$), BP parameters ($E_{\max}, \eta, \varepsilon_{\text{target}}$)

Output: Optimized parameters $\{W^*, \theta^*\}$, Prediction metrics (MAPE, R^2)

`// Stage 1: Genetic Algorithm for Initial Weights`

Initialize population P_0 (chromosomes represent weights/thresholds);

Evaluate fitness $F = 1/\text{RMSE}$ for all chromosomes in P_0;

$chr^* \leftarrow$ best individual in P_0, $\quad t \leftarrow 1$;

while $t \leq T_{\max}$ ***and*** $\text{error}(chr^*) > \varepsilon_{\text{target}}$ **do**

  $P_{\text{sel}} \leftarrow \text{RouletteWheelSelect}(P_t, F_t)$;

  $P_{\text{new}} \leftarrow \text{Crossover}(P_{\text{sel}}, cr)$; `// Pairwise crossover`

  $P_{\text{new}} \leftarrow \text{Mutation}(P_{\text{new}}, pm, \alpha)$; `// Gene mutation`

  $P_{t+1} \leftarrow \text{Elitism}(P_{\text{new}}, chr^*)$; `// Keep best individual`

  Update fitness F_{t+1} and global optimum chr^*;

  $t \leftarrow t + 1$;

end

`// Stage 2: BP Neural Network Fine-tuning`

$\{W^*, \theta^*\} \leftarrow \text{Decode}(chr^*)$;

for $e = 1$ **to** $E_{\max}$ **do**

  $\hat{R} \leftarrow \text{ForwardProp}(X, W^*, \theta^*)$;

  $E \leftarrow \frac{1}{2}\sum(R - \hat{R})^2$;

  if $E < \varepsilon_{\text{target}}$ **then**

    break

  end

  Update $W^* \leftarrow W^* - \eta \frac{\partial E}{\partial W^*}$ and $\theta^* \leftarrow \theta^* - \eta \frac{\partial E}{\partial \theta^*}$;

end

return $\{W^*, \theta^*\}$, MAPE, R^2;

2.2. *CPSO for screen-printing process optimization*

The PSO algorithm [28] is a population-based evolutionary computation technique inspired by the information exchange and social behavior observed in bird flocks and fish schools. The core idea of PSO is to obtain the optimal solution through information sharing and cooperative interaction among individuals in a population. Owing to its ease of implementation and the small number of adjustable parameters, PSO has been widely applied in function optimization, neural network training, fuzzy system control, and engineering optimization [29–31].

For the optimization of screen-printing process parameters in thick-film resistors, there exists a complex nonlinear mapping relationship between process parameters and resistance values. To achieve precise control of the target resistance value, it is necessary to search for the optimal parameter combination within the given process parameter design space. Therefore, the PSO algorithm is adopted in this study to perform global optimization of process parameters. The velocity and position update equations of the particles are expressed as follows:

$$v_{ij}^{k+1} = wv_{ij}^{k} + c_1 r_1 \left(p_{ij}^{k} - x_{ij}^{k}\right) + c_2 r_2 \left(p_{gj}^{k} - x_{ij}^{k}\right), \tag{1}$$

$$x_{ij}^{k+1} = x_{ij}^{k} + v_{ij}^{k+1}. \tag{2}$$

In Equations (1) and (2), w is the inertia weight, c_1 and c_2 are the learning factors, and r_1 and r_2 are random numbers in the interval $[0,1]$. v_{ij}^k and x_{ij}^k denote the velocity and position of particle i in the jth dimension at the kth iteration, respectively, while p_{ij}^k and p_{gj}^k represent the individual best position and the global best position of particle i in the jth dimension at the kth iteration, respectively. The particle position corresponds to specific screen-printing process parameter variables, and its iterative movement toward the global optimum essentially reflects the search process in which different process parameter combinations approach the optimal resistance value.

The optimal position of a particle is evaluated by the objective function. In this study, the optimization objective is the resistance accuracy of thick-film resistors, namely, under the optimized process parameter combination, the deviation between the predicted resistance value and the target resistance value is minimized. Based on this, the objective function is constructed as follows:

$$\min f(X) = \left(g(X) - R_{\text{target}}\right)^2 \qquad \text{s.t. } X \in \Omega. \tag{3}$$

In Equation (3), f denotes the objective function, g denotes the resistance prediction function, X is the set of input process parameter features, R_{target} is the target value, and Ω is the design interval for process parameter optimization. The particle iteration direction is the direction in which the objective function value decreases.

According to Equation (1), w, c_1, and c_2 are all constants. During the optimization process, all particles in the swarm tend to move toward the current global best particle, resulting in reduced population diversity. In high-dimensional and multimodal optimization problems of thick-film resistor process parameters, this property may cause the algorithm to fall into local optima, thereby affecting the accuracy of the final optimization results. CPSO incorporates a nonlinear chaotic mapping function into the velocity update equation of particles [32]. Chaotic mapping is a class of nonlinear dynamical systems with high complexity and stochastic characteristics. It is highly sensitive to initial values and parameters and can generate seemingly irregular trajectories. Therefore, chaotic mapping exhibits nonlinearity, unpredictability, and sensitivity to initial conditions. Its formulation is given as follows:

$$x_{n+1} = f(x_n). \tag{4}$$

In Equation (4), x_n denotes the value at the nth iteration, x_{n+1} denotes the value at the $(n+1)$th iteration, and $f(x)$ denotes the specific form of the chaotic mapping, such as Logistic mapping, Tent mapping, and Sin mapping. The random number generated by chaotic mapping is expressed as:

$$r_n = \frac{x_n - \lfloor x_n \rfloor}{1 - \lfloor x_n \rfloor}. \tag{5}$$

In Equation (5), r_n denotes the nth random number, x_n denotes the nth iterative value of the chaotic mapping, and $\lfloor x_n \rfloor$ denotes the floor value of x_n. The introduction of this function aims to enhance the global search capability of the particle swarm algorithm.

In the process optimization of thick-film resistors, the CPSO algorithm with the introduced chaotic mechanism can perform a more comprehensive search over the entire process parameter design space Ω, enabling different particles corresponding to different process parameter combinations to maintain higher diversity, thereby improving the capability of locating the global optimal resistance solution. Ultimately, by coupling the CPSO algorithm with the GA-BP prediction model, efficient inverse design of the optimal screen-printing process parameter combination under the target resistance requirement is achieved.

3. Implementation details

3.1. Dataset

The fabrication process of thick-film resistors generally consists of three main stages, namely screen printing, high-temperature drying/sintering, and laser trimming. Among them, the screen-printing stage is used to form the resistor pattern on the substrate and can directly determine the geometric dimensions of the resistor, including its length, width, and thickness. The drying and sintering stage is responsible for solvent evaporation and microstructure evolution of the resistive film, thereby affecting the resistivity of the material. The laser trimming stage is mainly used to finely adjust the final resistance value after fabrication in order to meet the target specification.

In general, the resistance value of a thick-film resistor is jointly determined by its geometric dimensions and resistivity. The geometric dimensions are mainly controlled by the screen-printing process, whereas the resistivity is more strongly influenced by the drying and sintering conditions. Since the sintering process involves multiple factors, such as peak temperature and heating profile, and the influence of each factor on the final resistance is highly coupled and difficult to quantify, the drying and sintering conditions were kept fixed in this work. Accordingly, the screen-printing process was selected as the core optimization target.

Based on this engineering consideration, the input parameters of the present model were selected from the main controllable and recordable variables in the screen-printing stage. Specifically, stencil thickness, screen mesh count, printing angle, printing gap, printing speed, printing pressure, printing direction, and height compensation were chosen because they directly affect paste transfer, printed pattern formation, film thickness uniformity, and ultimately the final resistance value. The output variable is the final resistance value of the thick-film resistor. The definitions of the input variables are listed in Table 1.

Table 1. Inputs of the prediction model.

Input	Variable Name	Input	Variable Name
x_1 (μm)	Stencil thickness	x_5 (mm/s)	Printing speed
x_2	Screen mesh count	x_6 (MPa)	Printing pressure
x_3 (deg)	Printing angle	x_7	Printing direction
x_4 (mm)	Printing gap	x_8 (mm)	Height compensation

In this study, process data from an actual production line of thick-film resistors are used as the research object, aiming to improve the consistency and stability of resistance values through data-driven methods and to verify the effectiveness of the proposed GA-BP prediction model and CPSO-based process parameter optimization method.

The experimental data are obtained from production-line process records, which include multiple groups of resistance measurements under different screen-printing process parameter conditions.

Specifically, before data collection, the screen-printing fabrication process of thick-film resistors was systematically analyzed to identify the controllable factors affecting the final resistance value. Based on the process analysis, a design-of-experiments method was employed to determine the parameter ranges, parameter levels, and experimental combinations under practical process conditions and equipment constraints. According to the designed experimental scheme, thick-film resistor samples were fabricated on the actual production line by varying the controllable process parameters, and the corresponding resistance values were measured and recorded after fabrication. Therefore, the dataset used in this work was established through a systematic experimental procedure based on actual production conditions, which improves its credibility and representativeness.

3.2. BP neural network parameter settings

To establish the nonlinear mapping relationship between screen-printing process parameters and resistance values, a BP neural network is employed to construct the prediction model. According to the number of input variables and the required model complexity, the neural network is configured as a three-layer feedforward network, including an input layer, a single hidden layer, and an output layer. The number of neurons in the input layer is 8, corresponding to the eight screen-printing process parameters, and the number of neurons in the output layer is 1, corresponding to the predicted resistance value.

In the hidden layer, the tansig function is used as the activation function to enhance the model's ability to represent nonlinear relationships, while the purelin function is used in the output layer to achieve continuous value prediction. The network is trained using the Levenberg–Marquardt algorithm, which exhibits fast convergence speed and high training efficiency for small- and medium-sized datasets. The maximum number of training iterations is set to 1000, the error threshold is set to 10^{-4}, and the learning rate is 0.01. The loss function is the mean squared error (MSE). The detailed parameter settings of the BP neural network are listed in Table 2. A total of 4800 experimental datasets were obtained. Typically, 80% of the data (3744 samples) were used as the training set, while the remaining data were divided into a test set (10%, 526 samples) and a validation set (10%, 526 samples).

Table 2. Parameter settings of the BP neural network model.

Model Parameter	Setting
Number of input neurons	8
Number of hidden neurons	17
Hidden layer activation function	tansig
Number of output neurons	1
Output layer activation function	purelin
Number of iterations	1000
Number of network layers	3
Error threshold	10^{-4}
Learning rate	0.01
Training method	Levenberg–Marquardt
Loss function	MSE

3.3. GA parameter settings

Since traditional BP neural networks are sensitive to the initial weights and thresholds during training and may fall into local optima, GA is introduced in this study to optimize the initial weights and thresholds of the BP network. By leveraging the global search capability of GA, better initial network parameters can be found within a larger parameter space, thereby improving model training stability and prediction accuracy.

In the GA optimization process, real-number encoding is adopted to represent network weights and thresholds. The population size is set to 30 to balance search capability and computational complexity. The number of generations is set to 500 to ensure sufficient evolutionary iterations. The fitness function is defined as the reciprocal of the prediction error (1/RMSE), so that individuals with smaller prediction errors have higher fitness values. Unless otherwise specified, the hyperparameter settings used in this study were determined through extensive preliminary experiments during the development of the proposed method. By repeatedly testing different parameter combinations, we selected the final settings to achieve a good balance among convergence stability, prediction accuracy, optimization performance, and computational efficiency on the present dataset. The detailed parameter configuration is shown in Table 3.

Table 3. Parameter settings of the GA optimization algorithm.

Algorithm Parameter	Setting
Number of generations	500
Population size	30
Number of optimization variables	171
Optimization variable bounds	$[-1, 1]$
Encoding method	Real-number encoding
Selection function parameter	0.09
Crossover function parameter	2
Upper mutation probability	0.1
Lower mutation probability	0.01
Fitness evaluation	1/RMSE

3.4. CPSO parameter settings

After obtaining a high-accuracy resistance prediction model, the CPSO algorithm is further employed to optimize the screen-printing process parameters to obtain the optimal parameter combination satisfying the target resistance value. Compared with the conventional PSO algorithm, CPSO enhances the global search capability of the particle swarm by introducing a chaotic mapping mechanism, thereby reducing the risk of the algorithm being trapped in local optima.

In the algorithm implementation, the swarm size is set to 40, and the particle dimension is 8, corresponding to the eight screen-printing process parameters. The maximum number of iterations is set to 200 to balance computational efficiency and optimization performance. The cognitive factor and social factor are both set to 1.5 to maintain a proper balance between individual experience and group information. The inertia weight varies dynamically from 0.5 to 0.9 to improve the search capability at different stages. In addition, chaotic sequences are introduced to perturb particle positions by setting chaotic mapping parameters and iteration numbers, further enhancing the global optimization performance of the algorithm. The detailed parameter settings of CPSO are listed in Table 4.

Table 4. Parameter settings of the CPSO algorithm.

Algorithm Parameter	Setting
Swarm size	40
Particle dimension	8
Maximum number of iterations	200
Cognitive component	1.5
Social component	1.5
Inertia weight	0.5–0.9
Maximum velocity	3
Chaotic mapping parameter	4
Chaotic sequence dimension	8
Number of chaotic iterations	40

4. Results and discussion

4.1. Results of the GA-BP prediction model

Based on the GA-BP model parameters defined above, the neural network is trained and optimized using the training dataset to construct an accurate resistance prediction model for thick-film resistors. Subsequently, the model is validated using the test dataset. The MSE iteration during the training process is shown in Figure 3. The optimal MSE is achieved at the 13th iteration, at which point the training is terminated, with a value of 7.1075×10^{-4}, indicating that the training stops when the expected error requirement is satisfied.

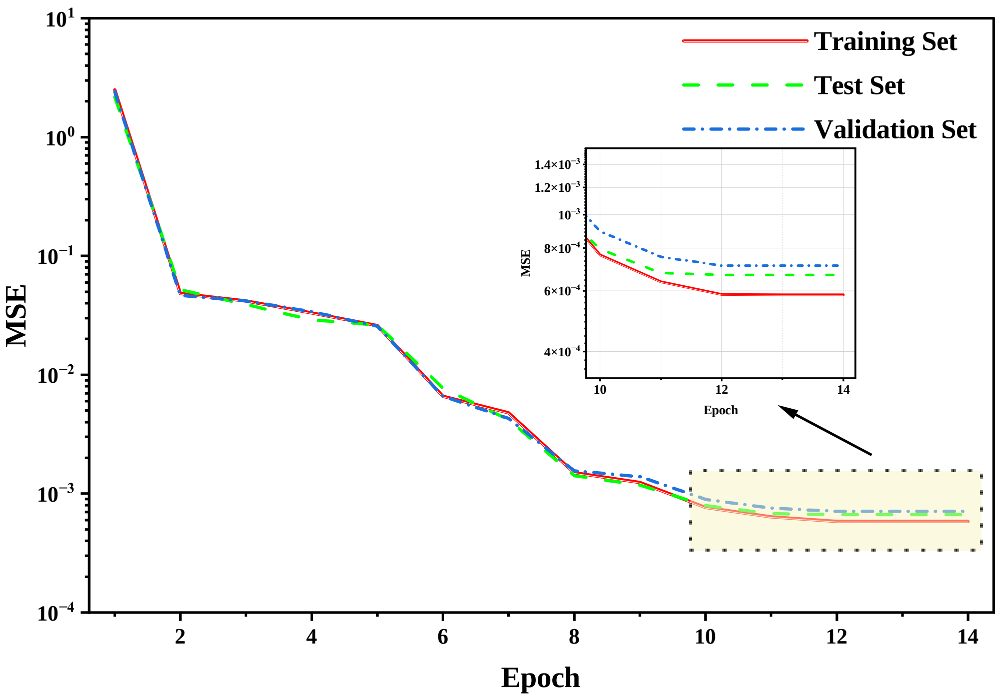

Figure 3. MSE iteration during model training.

To quantitatively evaluate the prediction results and model performance, two error metrics are adopted: MAPE and R^2. The GA-BP model achieves a MAPE of 2.72% on the training set and 3.09% on the test set. The R^2 values of the model on the training, test, and validation sets are 0.991, 0.991, and 0.988, respectively. These R^2 values are close to 1, indicating that the model has high fitting accuracy and stability. To further demonstrate the effectiveness of the proposed method, comparative experiments are conducted with the conventional BP neural network, response surface methodology (RSM), and linear regression (LR) model. As shown in Figure 4, the proposed GA-BP model achieves the best overall performance, with an R^2 value of 0.991 and a MAPE of 3.09%, outperforming the BP model ($R^2 = 0.923$, MAPE = 6.52%), the RSM model ($R^2 = 0.988$, MAPE = 3.23%), and the LR model ($R^2 = 0.889$, MAPE = 10.43%). In particular, compared with the conventional BP model, the GA-BP model yields both higher prediction accuracy and stronger generalization capability, confirming the effectiveness of introducing GA to optimize the initial weights and thresholds of the neural network. Although the RSM model also achieves relatively good performance, its accuracy is still slightly inferior to that of the proposed method, indicating that the nonlinear mapping between screen-printing parameters and resistance values cannot be fully characterized by a conventional quadratic response surface. Overall, these results confirm the effectiveness of the proposed GA-BP model for resistance prediction based on screen-printing parameters.

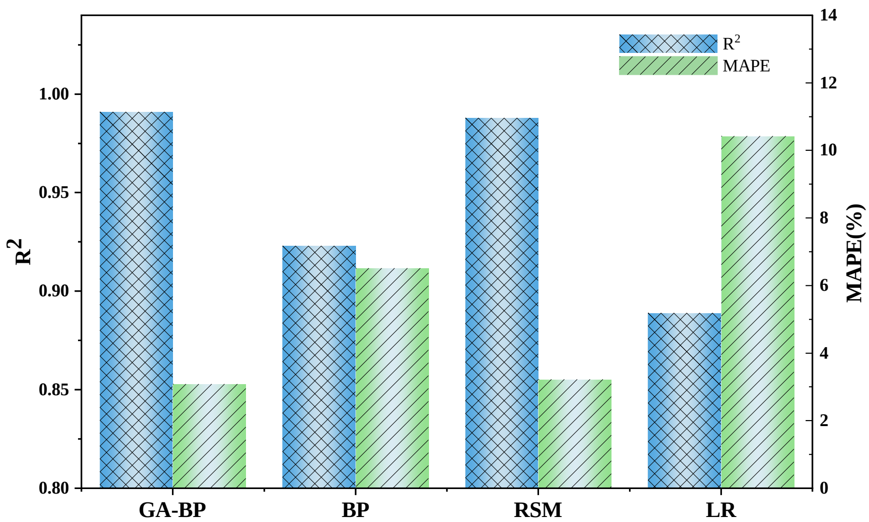

Figure 4. Comparison of R^2 and MAPE among GA-BP, BP, RSM, and LR models.

Figure 5 shows the comparison between predicted and actual values of the GA-BP model on the training and test sets. It can be observed that most data points are distributed near the ideal prediction line, indicating high fitting accuracy. Meanwhile, the distributions of the training and test datasets are generally consistent, demonstrating that the model has good generalization capability. In summary, the BP neural network optimized by a genetic algorithm exhibits higher accuracy in predicting the resistance of thick-film resistors and can effectively reduce the number of preliminary trial adjustments in the production process through accurate resistance prediction, thereby improving production efficiency.

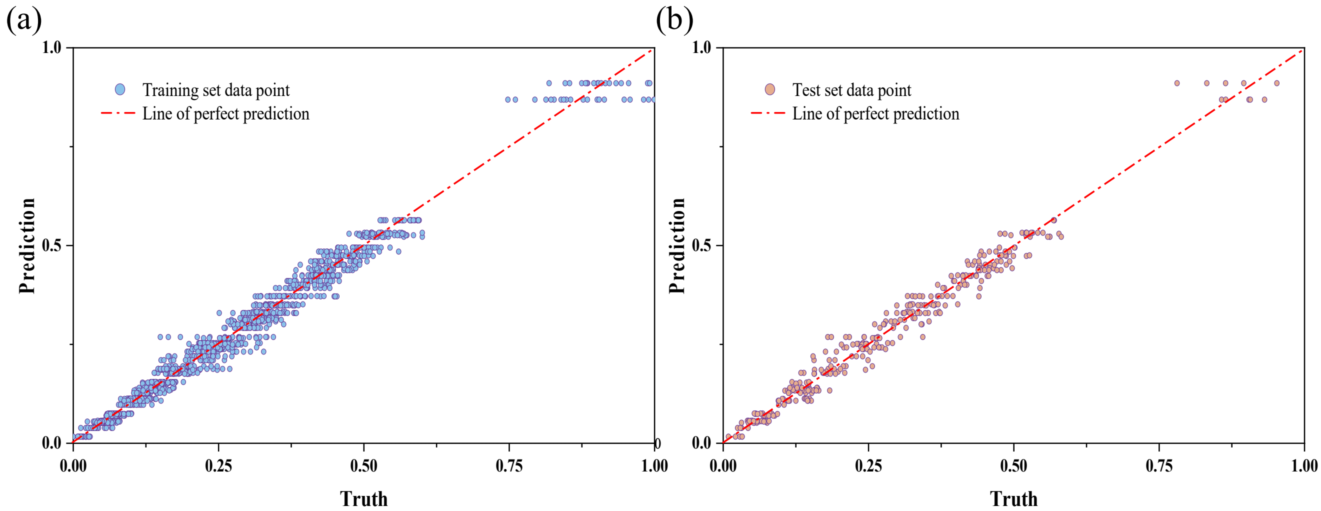

Figure 5. Comparison between predicted and actual values of the GA-BP model: **(a)** training set and **(b)** test set.

4.2. Results of the CPSO optimization model

Based on the established high-accuracy GA-BP resistance prediction model, the CPSO algorithm is applied to optimize the screen-printing process parameter window. First, the optimization search space Ω of the process parameters is defined, as shown in Table 5. The search ranges are determined according to commonly used production parameters and equipment constraints. In our implementation, one round of parameter optimization for a given target resistance takes approximately 2.38 s after the GA-BP model has been trained, indicating that the proposed method can provide efficient parameter recommendations for practical fabrication processes.

Table 5. Search space of screen-printing process parameters.

Parameter	Search Space	Parameter	Search Space
x_1	$\{30,40,50\}$	x_5	$[80,200]$
x_2	$\{325,400\}$	x_6	$[2.4,4.8]$
x_3	$\{45,60\}$	x_7	$\{0,90\}$
x_4	$[2,4]$	x_8	$[5,15]$

Based on the CPSO parameter settings shown in Table 4, the CPSO algorithm is applied to perform inverse optimization of screen-printing process parameters using the GA-BP model as the fitness function. The nominal resistance value of the electronic paste is taken as the optimization target, which is defined as $R_{\text{target}} = 115\ \Omega$. The objective function values during the CPSO iteration process are shown in Figure 6, which meet the predefined threshold.

After optimization, four groups of process parameters closest to the target value are selected as recommended results, as shown in Table 6. The standard group corresponds to the empirical parameter settings in production, with a predicted resistance of 136.03 Ω, which is significantly higher than R_{target}. The optimized groups (Opt-1 to Opt-4) are obtained by CPSO and represent the optimal parameter window.

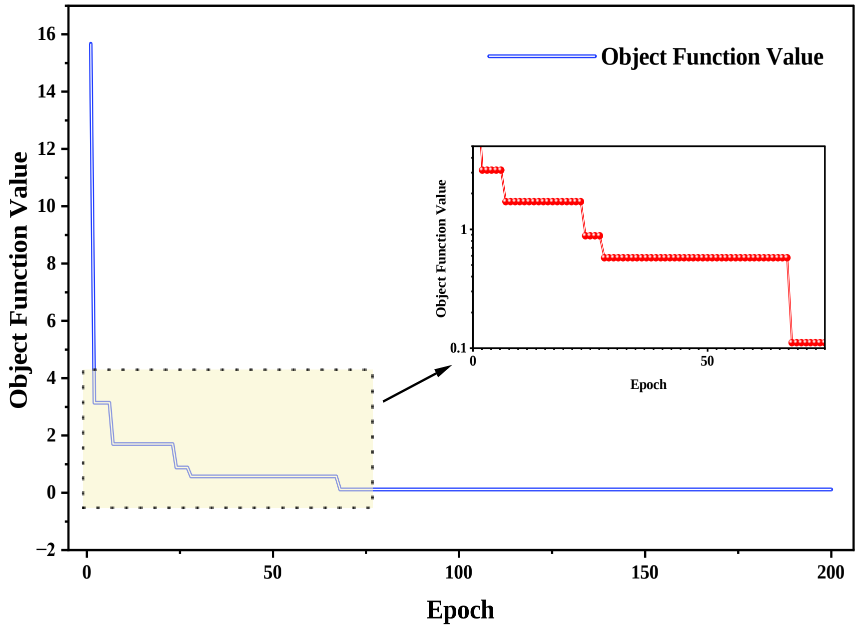

Figure 6. Objective function values of CPSO.

Table 6. Optimized screen-printing process parameter combinations.

Group	x_1	x_2	x_3	x_4	x_5	x_6	x_7	x_8	**Predicted** (Ω)
Standard	40	325	45°	2.7	100	4.4	0°	10.15	136.03
Opt-1	50	325	45°	2.3	120	4.1	0°	9.98	115.47
Opt-2	50	325	45°	2.32	158	4.0	0°	9.98	115.07
Opt-3	50	325	45°	2.34	130	4.2	0°	10.05	115.01
Opt-4	50	325	45°	2.3	115	4.4	0°	10.00	115.75

To verify the effectiveness of the proposed optimization strategy, experimental fabrication is conducted, and the deviation between the actual resistance and R_{target} is shown in Table 7. The results indicate that the standard group deviates significantly from the target value, with a deviation of 15.32%, whereas all optimized groups achieve deviations within 5%, demonstrating superior optimization performance and reduced trial production requirements. In particular, the minimum deviation is reduced to 0.459%, and most optimized results are concentrated within a narrow range of 0.459%–4.371%, indicating improved resistance accuracy and stability. Compared with the standard group, the optimization results exhibit a substantial reduction in deviation, confirming the effectiveness and reliability of the proposed method.

Table 7. Experimental validation results of optimized parameters.

Group	**Actual Resistance** (Ω)	**Deviation**
Standard	132.62	15.32%
Opt-1	116.00	0.459%
Opt-2	117.42	2.042%
Opt-3	116.93	1.669%
Opt-4	120.81	4.371%

To further verify the model, target resistance values of 120 Ω, 130 Ω, and 140 Ω were also tested. The optimized parameter combinations are listed in Table 8. It can be observed that the predicted resistance values (119.06 Ω, 131.31 Ω, and 140.05 Ω) are in close agreement with the corresponding target values, demonstrating the effectiveness of the proposed optimization method across different design objectives.

To reduce the influence of experimental randomness, two groups of samples are fabricated for each target resistance value according to the parameter distributions in Table 8. The validation results are shown in Figure 7. The measured resistance values are highly consistent with the predicted results, and all deviations are controlled within ±2.1%, indicating high design accuracy and process stability. In addition, the mean prediction error for each group remains at a low level, further confirming the reliability and generalization capability of the proposed model.

Table 8. Optimization results under different target resistances.

Group	x_1	x_2	x_3	x_4	x_5	x_6	x_7	x_8	Predicted (Ω)
1	50	325	45°	2.3	160	4.0	10.03	90°	119.06
2	50	325	45°	2.64	150	4.3	10.35	90°	131.31
3	50	325	45°	2.5	164	4.6	10.45	0°	140.05

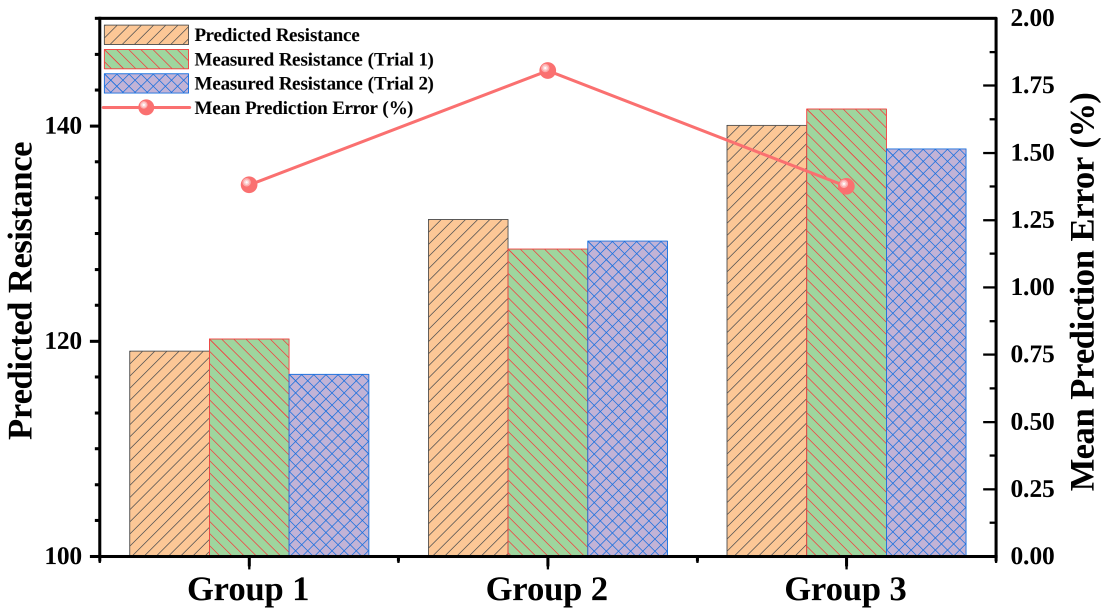

Figure 7. Validation results under different target resistances.

4.3. Analysis of process parameter influence

To quantitatively evaluate the influence of each process parameter on the resistance prediction, a gradient boosting decision tree (GBDT)-based feature importance analysis was further carried out, and the results are shown in Figure 8. In the GBDT model, each regression tree is constructed by recursively selecting the feature that can achieve the largest reduction in the loss function at each splitting node. Therefore, when a feature is repeatedly selected for node splitting and leads to a larger reduction in prediction error, it is regarded as having higher importance in the prediction task. Specifically, the importance score of the

ith feature is calculated by accumulating its contribution to the loss reduction over all splitting nodes and all regression trees, which can be expressed as

$$I_i = \sum_{t=1}^{T} \sum_{s \in S_i^{(t)}} \Delta L_s^{(t)},$$

where T is the total number of trees in the GBDT model, $S_i^{(t)}$ denotes the set of splitting nodes in the tth tree that use the ith feature, and $\Delta L_s^{(t)}$ represents the reduction in the loss function contributed by that split. The contribution percentage of each parameter is then obtained by normalizing its importance score as

$$C_i = \frac{I_i}{\sum_{j=1}^{n} I_j} \times 100\%,$$

where n is the total number of input features. In this way, the reported contribution percentages in Figure 8 reflect the relative importance of different process parameters in the trained GBDT model.

The results indicate that height compensation is the most significant factor affecting resistance, followed by stencil thickness and printing gap. This is consistent with practical production experience, where stencil thickness determines the initial resistance range, and height compensation is used for fine control. The findings provide important guidance for subsequent model optimization and experimental design.

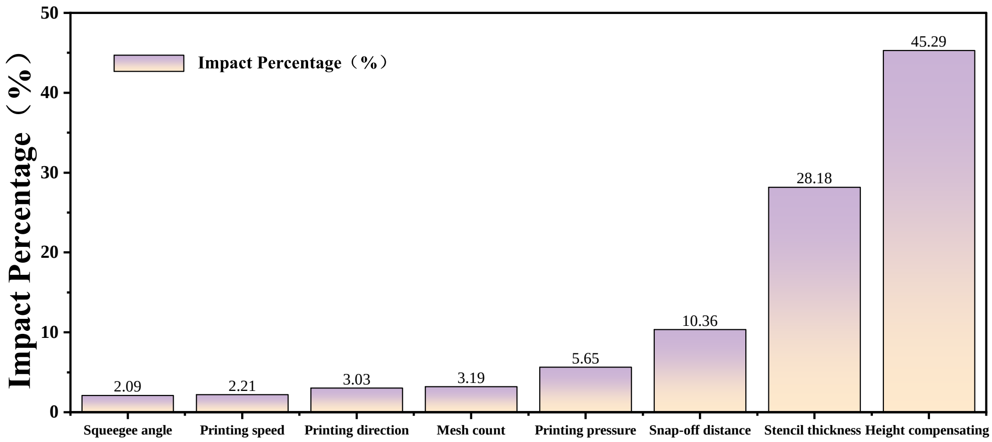

Figure 8. Contribution of screen-printing process parameters.

5. Conclusion

This study proposes a data-driven process optimization method that integrates a GA-BP prediction model with a CPSO optimization algorithm for screen-printing process optimization of thick-film resistors. The effectiveness of the proposed approach is systematically verified through experimental analysis. The results demonstrate that the BP neural network optimized by a genetic algorithm can effectively capture the complex nonlinear relationship between screen-printing process parameters and resistance values, significantly improving the prediction accuracy and stability of the model. On this basis, by introducing the chaotic particle swarm optimization algorithm to perform global search of process parameters, parameter inverse design oriented toward the target resistance value is achieved. Experimental results show that, compared with traditional empirical parameter settings, the optimized process combinations can effectively control the resistance deviation within 5%, substantially reducing the number of trial productions and improving process development efficiency. In addition, the parameter contribution analysis based on the model reveals that height compensation and stencil thickness play dominant roles in resistance regulation. This finding is highly consistent with practical production experience, further validating the physical rationality and interpretability of the proposed model.

Data availability statement

The data that support the findings of this study are not publicly available due to commercial confidentiality, but are available from the corresponding author upon reasonable request.

Declaration of generative AI and AI-assisted technologies

During the preparation of this manuscript, the authors used generative AI tools only to improve language and readability. Specifically, the authors used ChatGPT for language polishing only. The authors take full responsibility for the content of the manuscript.

Acknowledgments

Funding: This work was funded by the Jiangsu Provincial Key Research and Development Program with grant number BE2023818, the National Natural Science Foundation of China with grant numbers 62404103, 62271258, and 62401261, Basic Research Program of Jiangsu with grant numbers BK20243046 and BK20253062, Fundamental Research Funds for the Central Universities with grant number 30924012001, and Chinese Institute of Electronics (CIE)-Smartchip Research Fund with grant number 2023-003.

Authors' contribution

Conceptualization, Yu Sun, Xingyao Zhang, and Wenhua Gu; methodology, Yu Sun and Youyang Wang; software, Yu Sun and Xingyao Zhang; validation, Yu Sun, Jiani Xue, and Xingyao Zhang; formal analysis, Yu Sun; investigation, Yu Sun and Jiani Xue; resources, Xiyi Liao and Wenhua Gu; data curation, Yu Sun and Youyang Wang; writing—original draft preparation, Yu Sun, Jiani Xue, and Youyang Wang; writing—review and editing, Yu Sun, Youyang Wang, and Wenhua Gu; visualization, Yu Sun, Jiani Xue; supervision, Wenhua Gu; project administration, Xiyi Liao and Wenhua Gu; funding acquisition, Youyang Wang and Wenhua Gu. All authors have read and agreed to the published version of the manuscript.

Conflicts of interest

Wenhua Gu holds the position of Associate Editor for *Interdiscipline* and has not peer reviewed or made any editorial decisions for this paper. The authors declare that they have no known competing financial interests or personal relationships that could have appeared to influence the work reported in this paper.

References

[1] Coté RE, Bouchard RJ. Thick-film technology. In *Electronic Ceramics*, 1st ed. London: Taylor Francis Group, 2020. pp. 307–370.

[2] Reissing TC. An overview of today's thick-film technology. *Proc. IEEE* 1971, 59(10):1448–1454.

[3] Sumida T. Recent advances in thick-film resistors and target applications [passive components]. *IEEE Power Electron. Mag.* 2022, 9(1):70–72.

[4] Sun Y, Li L, Lin H, Yu Z, Huang M, *et al.* Attenuators using thin film resistors for RF application. In *Proceedings of 2008 International Conference on Electronic Packaging Technology and High Density Packaging*, Shanghai, China, July 28–31, 2008, pp. 1–3.

[5] Szczepański Z. Miniature thick film resistors for microwave integrated circuits. *Act. Pass. Electron. Compon.* 1991, 14(3):119–127.

[6] Aleksandrova MP, Andreev SK. Design methodology and technological flow of screen-printed thick-film sensors. *IEEE Sens. J.* 2021, 22(11):10126–10136.

[7] Fromm E. A thick-film hybrid implantable telemeter. *IEEE Eng. Med. Biol. Mag.* 2009, 2(1):38–41.

[8] Uhlig P, Serwa A, Müller J, Gutzeit N, Schwanke D, *et al.* LTCC resistors–the influence of production conditions on the absolute value and its reproducibility. In *Proceedings of 2018 IMAPS Nordic Conference on Microelectronics Packaging (NordPac)*, Oulu, Finland, June 12–14, 2018, pp. 61–66.

[9] Swiecinski K, Ihle M, Jurk R, Dietzen E, Partsch U, *et al.* Aerosol jet printing of two component thick film resistors on LTCC. *J. Microelectron. Electron. Packag.* 2013, 10(3):109–115.

[10] Dolden ED. Fundamental investigations into screen printing. Doctoral Thesis, University of Leeds, 2005.

[11] Owczarek JA, Howland FL. A study of the off-contact screen printing process. I. Model of the printing process and some results derived from experiments. *IEEE Trans. Compon. Hybrids Manuf. Technol.* 2002, 13(2):358–367.

[12] Koo BK. Effect of screen printing and sintering conditions on properties of thick film resistor on AlN substrate. *J. Korean Ceram. Soc.* 2014, 51(4):344–349.

[13] Leven SS. Proper optimization of the thick-film process for TCR and sheet resistivity. *Int. J. Hybrid Microelectron.* 1981, 4:40–41.

[14] Soyucayli S. Integrated design and manufacturing modeling of performance and variability for screen printed resistors in LTCC circuit technology. Doctoral Thesis, Massachusetts Institute of Technology, 1997.

[15] Pan J, Tonkay GL, Quintero A. Screen printing process design of experiments for fine line printing of thick film ceramic substrates. *J. Electron. Manuf.* 1999, 9(3):203–213.

[16] Horvath E, Torok A, Ficzere P, Zador I, Racz P. Optimisation of computer-aided screen printing design. *Acta Polytech. Hung.* 2014, 11(8):29–44.

[17] Choi SA, Youn JT, Mok JS, Koo CW. Computer simulation of ink transfer in the different printing speed and ink viscosity in the screen printing. *J. Korean Graph. Arts Commun. Soc.* 2011, 29(1):75–83.

[18] Sharma P, Dadheech P, Aneja N, Aneja S. Predicting agriculture yields based on machine learning using regression and deep learning. *IEEE Access* 2023, 11:111255–111264.

[19] Jiao Y, Liu Z, Wan P, Cui X, Wei Y, *et al.* Physics-constrained neural network-based compact modeling of displacement damage for AlGaN/GaN HEMTs. *IEEE Trans. Nucl. Sci.* 2025, 72(10):3364–3374.

[20] Liu S, Duan X, Wang S, Zhang J, Hao Y. Optimization of dual field plate AlGaN/GaN HEMTs using artificial neural networks and particle swarm optimization algorithm. *IEEE Trans. Device Mater. Reliab.* 2023, 23(2):204–210.

[21] Cheng X, Zhang P, Zhou Y, Sun D, Gu W, *et al.* A bidirectional deep learning approach for designing MEMS sensors. *IEEE Trans. Comput.-Aided Des. Integr. Circuits Syst.* 2022, 42(5):1610–1617.

[22] Zhang P, Cheng X, Zhou Z, Zhang Q, Gu W, *et al.* An artificial neural network method for high-accurate and high-efficient MEMS pressure sensor design. *IEEE Sens. J.* 2022, 22(21):20585–20592.

[23] Mohamad ET, Armaghani DJ, Momeni E, Yazdavar AH, Ebrahimi M. Rock strength estimation: a PSO-based BP approach. *Neural Comput. Appl.* 2018, 30(5):1635–1646.

[24] Zhu C, Zhang J, Liu Y, Ma D, Li M, *et al.* Comparison of GA-BP and PSO-BP neural network models with initial BP model for rainfall-induced landslides risk assessment in regional scale: a case study in Sichuan, China. *Nat. Hazards* 2020, 100(1):173–204.

[25] Shariati M, Mafipour MS, Mehrabi P, Bahadori A, Zandi Y, *et al.* Application of a hybrid artificial neural network-particle swarm optimization (ANN-PSO) model in behavior prediction of channel shear connectors embedded in normal and high-strength concrete. *Appl. Sci.* 2019, 9(24):5534.

[26] Marakhimov A, Khudaybergenov K. Convergence analysis of feedforward neural networks with backpropagation. *Convergence* 2019, 6:6–2019.

[27] Alhijawi B, Awajan A. Genetic algorithms: theory, genetic operators, solutions, and applications. *Evol. Intell.* 2024, 17(3):1245–1256.

[28] Kennedy J, Eberhart R. Particle swarm optimization. In *Proceedings of ICNN'95 International Conference on Neural Networks*, Perth, Australia, November 27–December 1, 1995, pp. 1942–1948.

[29] Khan RA, Yang S, Fahad S, Khan SU. A modified particle swarm optimization with a smart particle for inverse problems in electromagnetic devices. *IEEE Access* 2021, 9:99932–99943.

[30] Shami TM, El-Saleh AA, Alswaitti M, Al-Tashi Q, Summakieh MA, *et al.* Particle swarm optimization: a comprehensive survey. *IEEE Access* 2022, 10:10031–10061.

[31] Açıkkar M, Altunkol Y. A novel hybrid PSO- and GS-based hyperparameter optimization algorithm for support vector regression. *Neural Comput. Appl.* 2023, 35(27):19961–19977.

[32] Liu B, Wang L, Jin Y, Tang F, Huang D. Improved particle swarm optimization combined with chaos. *Chaos Solitons Fractals* 2005, 25(5):1261–1271.